Monthly Notices
of the
ROYAL ASTRONOMICAL SOCIETY

MNRAS **474,** 1526–1537 (2018)
Advance Access publication 2017 November 2

doi:10.1093/mnras/stx2840

On the internal structure of the current sheet in the pulsar wind

V. V. Prokofev,[1]★ L. I. Arzamasskiy[2]★ and V. S. Beskin[1,3]★

[1]*Moscow Institute of Physics and Technology, Dolgoprudny, Institutsky per., 9, Moscow region, 141700, Russia*
[2]*Department of Astrophysical Sciences, Peyton Hall, Princeton University, Princeton, NJ 08544, USA*
[3]*P.N.Lebedev Physical Institute, Leninsky prosp., 53, Moscow, 119991, Russia*

Accepted 2017 October 31. Received 2017 October 31; in original form 2017 January 31

ABSTRACT

We investigate the internal structure of the current sheet in the pulsar wind within force-free and two-fluid MHD approximations. Within the force-free approximation we obtain general asymptotic solution of the Grad–Shafranov equation for quasi-spherical pulsar wind up to the second order in small parameter $\varepsilon = (\Omega r/c)^{-1}$. The solution allows an arbitrary latitudinal structure of the radial magnetic field, including that obtained in the numerical simulations of oblique rotators. It is also shown that the shape of the current sheet does not depend on the latitudinal structure. For the internal region of the current sheet outside the fast magnetosonic surface where the force-free approximation is not valid we use two-fluid MHD approximation. Carrying out calculations in the comoving reference frame, we succeed in determining intrinsic electric and magnetic fields of a sheet. It allows us to analyse time-dependent effects which were not investigated up to now. In particular, we estimate the efficiency of the particle acceleration inside the sheet. Finally, after investigating the motion of individual particles in the time-dependent current sheet, we find the width of the sheet and its time evolution self-consistent.

Key words: pulsars: general.

1 INTRODUCTION

Particle acceleration in compact astrophysical objects is the classical problem of modern astrophysics. Indeed, high-energy radiation in the GeV and even TeV energy band is the smoking gun of the existence of the relativistic particles with characteristic Lorentz factors γ up to 10^4–10^5 (Levinson 2000; Aharonian et al. 2007).

Radio pulsars are thought to be the most effective accelerators in space. Indeed, fast rotation of a neutron star (radius $R \sim 10$–15 km and periods $P \sim 1$ s for ordinary pulsars) with surface magnetic field $B_0 \sim 10^{11}$–10^{13} G (and even 10^{13}–10^{15} G for magnetars) inevitably results in the generation of the large enough electric field $E \sim (\Omega R_0/c)B_0$. Here $\Omega = 2\pi/P$ is the neutron star angular velocity and R_0 is the effective radius of the 'central engine'; for radio pulsars $R_0 \approx (\Omega R/c)^{1/2}R$ is the polar cap radius. The energetics of radio pulsars is determined by the potential drop $V_{\rm tot} \sim ER_0$.

To determine the specific realization of the effective particle acceleration self-consistently, it is necessary to know in detail the structure of the neutron star magnetosphere and the pulsar wind. Important analytical results were already obtained in the first quarter of the century after radio pulsars were discovered. In particular, the role of the process of the quantum-mechanical particle creation was clarified (Sturrock 1971; Ruderman & Sutherland 1975; Arons 1981). It showed the very possibility of the quasi-radial magnetized wind transporting electromagnetic energy to infinity (Michel 1973; Blandford 1975; Bogovalov 1999). It also predicted the full screening of magnetodipole radiation by plasma filling the neutron star magnetosphere (Beskin, Gurevich & Istomin 1993). Later these results were confirmed with numerical simulations of axisymmetric (Contopoulos, Kazanas & Fendt 1999; Timokhin 2006; Gruzinov 2005; Komissarov 2006) as well as inclined magnetosphere (Kalapotharakos, Contopoulos & Kazanas 2012; Tchekhovskoy, Spitkovsky & Li 2013).

As a result, at large enough distance from a neutron star $r \gg R_{\rm L}$ ($R_{\rm L} = c/\Omega$ is the radius of the light cylinder) the theory predicts the quasi-radial outflow of the relativistic electron–positron plasma along the poloidal magnetic field. As the total flux of the magnetic field through the whole sphere is to vanish, such a structure is to contain the current sheet separating outgoing and ingoing magnetic fluxes. Up to the light cylinder the energy is mainly transported by the electromagnetic field (i.e. by the flux of the Poynting vector $\mathbf{S} = (c/4\pi)\boldsymbol{E} \times \boldsymbol{B}$), but somewhere at larger distances the electromagnetic energy flux is to be transferred into the particle energy. Actually, the mechanism of this transformation is the main subject of the particle acceleration theory. Up to now it remains an open question as the ideal MHD predicts very ineffective particle acceleration for quasi-radial outflow (Tomimatsu 1994; Beskin, Kuznetsova & Rafikov 1998).

★ E-mails: vadprokofev@gmail.com (VVP); leva@astro.princeton.edu (LIA); beskin@lpi.ru (VSB)

Clearly, for the MHD outflow to exist, the electric field $\boldsymbol{E}$ has to be smaller than the magnetic field $\boldsymbol{B}$. In the pulsar wind it can take place only if the total electric current I flowing in the magnetosphere (and producing toroidal magnetic field B_φ) is large enough so that at the light cylinder the toroidal magnetic field $B_\varphi \approx 2I/R_{\rm L}c$ becomes as large as the electric field. Indeed, both B_φ and E diminish with the distance as r^{-1} (and, accordingly, $S \propto r^{-2}$). As the poloidal magnetic field $B_{\rm p}$ for quasi-spherical structure decreases much faster ($B_{\rm p} \propto r^{-2}$), the very MHD approximation $E < B$ can be fulfilled only if the total electric current I circulating in the pulsar magnetosphere is as large as the so-called Goldreich–Julian current

$$I_{\rm GJ} = \pi R_0^2 j_{\rm GJ}^{\rm A}, \tag{1}$$

where

$$j_{\rm GJ}^{\rm A} = \frac{\Omega B}{2\pi} \tag{2}$$

is the amplitude of the Goldreich–Julian current density.

Here it is necessary to stress one important point. The definition of the Goldreich–Julian charge density

$$\rho_{\rm GJ} = -\frac{\boldsymbol{\Omega B}}{2\pi c} \tag{3}$$

contains the factor $\cos\theta_{\rm m}$, where $\theta_{\rm m}$ is the angle between the vectors $\boldsymbol{\Omega}$ and $\boldsymbol{B}$. As a result, for condition (1) to be fulfilled for large enough inclination angles χ between $\boldsymbol{\Omega}$ and the neutron star magnetic moment $\mathbf{m}$, the current density j should be larger than the local GJ current density $j_{\rm GJ} = \rho_{\rm GJ}c$ near magnetic poles where $\theta_{\rm m} \sim \chi$, and

$$j_{\rm GJ} \approx \frac{3}{2}\frac{\Omega B}{2\pi}\cos\theta. \tag{4}$$

Thus, for quasi-radial MHD outflow to exist, the pair creation mechanism has to support large enough longitudinal current $j > j_{\rm GJ}$ (4). At present, most scientists believe in this model (see e.g. Timokhin & Arons 2013), and here we follow this point of view as well. On the other hand, effective particle acceleration can be realized if the particle generation mechanism cannot support large enough longitudinal current j. It can take place in the vicinity of the so-called light surface $E = B$, which inevitablly appears outside the light cylinder for $j < j_{\rm GJ}$ (Beskin et al. 1993; Beskin & Rafikov 2000). Recently, the possible existence of such effective particle acceleration region was demonstrated by analysing the TeV time-dependent radiation of the Crab pulsar (Aharonian, Bogovalov & Khangulyan 2012).

Returning to standard model of the pulsar wind, let us recall that it contains 'striped' current sheet separating ingoing and outgoing magnetic fluxes. This current sheet was predicted analytically (Coroniti 1990; Michel 1994; Bogovalov 1999) and later was confirmed in numerous force-free (Contopoulos et al. 1999; Spitkovsky 2006; Kalapotharakos et al. 2012), MHD (Komissarov 2006; Tchekhovskoy, McKinney & Narayan 2009) and even PIC (Cerutti et al. 2015) simulations.[1] And it has long been understood that this current sheet can be the domain of very effective particle acceleration (Lyubarsky & Kirk 2001a; Zenitani & Hoshino 2007; Arons 2012; Contopoulos, Kalapotharakos & Kazanas 2014). On the other hand, the self-consistent model of the internal structure of this 'striped' current sheet was not constructed.

The paper is organized as follows. We start with the discussion of force-free asymptotic behaviour of the pulsar wind in Section 2. Here we obtain simple asymptotic solution of the Grad–Shafranov equation for quasi-spherical pulsar wind. In particular, this solution can describe the latitudinal structure of the radial magnetic field obtained numerically for the oblique rotator (Tchekhovskoy, Philippov & Spitkovsky 2016). We also show that the shape of the current sheet does not depend on the latitudinal structure. Then in Section 3 we determine the main properties of the internal regions of a current sheet where the force-free approximation is not valid. Using two-fluid MHD approximation and carrying out calculations in the comoving reference frame we determine electric and magnetic field structures as well as the velocity component perpendicular to the sheet. This allows us to estimate the efficiency of particle acceleration. After that we find the self-consistent solution for the current sheet evolution. Section 4 is devoted to numerical simulation which, as will be shown, fully support our analytical asymptotic solutions. Finally, in Section 5 we discuss possible astrophysical applications of our consideration.

2 FORCE-FREE ASYMPTOTIC BEHAVIOUR OF THE PULSAR WIND

2.1 Basic equations

In this section, we discuss the asymptotic behaviour of the pulsar wind using well-known approach of the so-called *pulsar equation* (Mestel 1973; Okamoto 1974)

$$-\left(1-\frac{\Omega_{\rm F}^2\varpi^2}{c^2}\right)\nabla^2\Psi + 2\frac{1}{\varpi}\frac{\partial\Psi}{\partial\varpi} + \frac{\varpi^2\Omega_{\rm F}}{c^2}(\nabla\Psi)^2\frac{{\rm d}\Omega_{\rm F}}{{\rm d}\Psi} - \frac{16\pi^2}{c^2}I\frac{{\rm d}I}{{\rm d}\Psi} = 0. \tag{5}$$

This equation resulting directly from Maxwell equations describes axisymmetric stationary electromagnetic fields,

$$\boldsymbol{E} = -\frac{\Omega_{\rm F}}{2\pi c}\nabla\Psi, \tag{6}$$

$$\boldsymbol{B} = \frac{\nabla\Psi\times\mathbf{e}_\varphi}{2\pi\pi r\sin\theta} - \frac{2I}{cr\sin\theta}\mathbf{e}_\varphi \tag{7}$$

within the force-free approximation. Here $\Psi = \Psi(r,\theta)$ is the magnetic flux, and two integrals of motion $\Omega_{\rm F} = \Omega_{\rm F}(\Psi)$ and $I = I(\Psi)$ are the so-called field angular velocity (more exactly, the angular velocity of a test charged particle drifting in the crossed electromagnetic fields) and the total current inside the magnetic tube, respectively. Below, for simplicity, we consider the case $\Omega_{\rm F} = \Omega$ only. It corresponds to the fast enough rotation of the neutron star when the potential drop in the inner gap $V_{\rm gap}$ is much smaller than the maximum value $V_{\rm tot}$.

The first solution of the pulsar, equation (5), containing radial wind was obtained by Michel (1973). He demonstrated that the 'split monopole' magnetic field corresponding to magnetic flux,

$$\Psi(r,\theta) = \Psi_{\rm tot}(1-\cos\theta), \qquad \theta < \pi/2, \tag{8}$$

$$\Psi(r,\theta) = \Psi_{\rm tot}(1+\cos\theta), \qquad \theta > \pi/2 \tag{9}$$

is the exact solution of the pulsar equation if the additional relation

$$4\pi I(\Psi) = \Omega_{\rm F}\left(2\Psi - \Psi^2/\Psi_{\rm tot}\right) \tag{10}$$

holds. In this case

$$B_r = B_{\rm L}\frac{R_{\rm L}^2}{r^2}\,{\rm sign}(\cos\theta), \tag{11}$$

[1] Nowhere any restrictions on the longitudinal current were imposed.

$$B_\varphi = E_\theta = -B_{\rm L}\frac{R_{\rm L}}{r}\sin\theta\,{\rm sign}(\cos\theta), \tag{12}$$

where $B_{\rm L} = B_{\rm p}(R_{\rm L}, \pi/2)$. This solution describing the axisymmetric case is called the 'split-monopole' one as it contains the current sheet in the equatorial plane separating ingoing and outgoing magnetic fluxes.

Later Ingraham (1973) found more general asymptotic solution, i.e. the solution in the limit $r \to \infty$. He has shown that in this limit an arbitrary function $\Psi = \Psi(\theta)$ remains the solution of the pulsar equation (5) if

$$4\pi I(\theta) = \Omega_{\rm F}\sin\theta\,\frac{{\rm d}\Psi}{{\rm d}\theta}. \tag{13}$$

According to equation (7), this implies that in the asymptotic limit $r \to \infty$ any θ-dependence of the poloidal magnetic field $B_{\rm p} = B_{\rm p}(\theta)$ can be realized. Here we have to stress that relation (3) for charge density remains true for monopole structure (11)–(12) only. In general case,

$$\rho_{\rm e} = -\frac{\Omega_{\rm F}}{4\pi\sin\theta}\,\frac{\rm d}{{\rm d}\theta}\left(\sin\theta\frac{{\rm d}\Psi}{{\rm d}\theta}\right). \tag{14}$$

As one can easily check using equations (6)–(7), both conditions (10) and (13) correspond to the clear relation $E_\theta = B_\varphi$.

Finally, it was found that the appropriate solution can be constructed for the oblique rotator as well. According to Bogovalov (1999), the 'inclined split monopole'

$$B_{\rm p} = B_{\rm L}\frac{R_{\rm L}^2}{r^2}\,{\rm sign}(\Phi), \tag{15}$$

$$B_\varphi = E_\theta = -B_{\rm L}\frac{R_{\rm L}}{r}\sin\theta\,{\rm sign}(\Phi), \tag{16}$$

where now

$$\Phi = \cos\theta\cos\chi - \sin\theta\sin\chi\cos\left[\varphi - \Omega\left(t - r/c\right)\right], \tag{17}$$

and χ is the inclination angle, is the exact solution of the pulsar equation as well. In the polar regions $\theta < \pi/2 - \chi$ and $\theta > \pi/2 + \chi$ this solution coincides with the time-independent Michel solutions (11)–(12), but in the equatorial region $\pi/2 - \chi < \theta < \pi/2 + \chi$ all the field components change the signs at the current sheet locating at the position $\Phi = 0$.

2.2 Asymptotic behaviour

In this section we are going to generalize the solutions mentioned above to substantiate the result of numerical simulation. Indeed, as shown by Tchekhovskoy et al. (2016), for large enough inclination angle $\chi > 30^\circ$ the φ-average poloidal magnetic field depends on the angle θ as

$$\langle B_{\rm p}\rangle_\varphi \propto \sin\theta. \tag{18}$$

For this reason, the structure of the solution with θ-dependent poloidal magnetic field (13) is to be considered in more detail.

As we are mainly interested in the asymptotic behaviour $r \gg R_{\rm L}$, one can search a solution of the pulsar equation (5) in the form

$$\Psi(r,\theta) = \sum_{n=0}^{\infty}\Psi_n(\theta)\left(\frac{R_{\rm L}}{r}\right)^{2n}{\rm sign}(\cos\theta). \tag{19}$$

As was already stressed, the function $\Psi_0(\theta)$ describing the asymptotic magnetic field can be arbitrary if the condition (13), $4\pi I(\theta) = \Omega_{\rm F}\sin\theta\,{\rm d}\Psi_0/{\rm d}\theta$ holds. According to equations (6)–(7), we obtain in the zero approximation

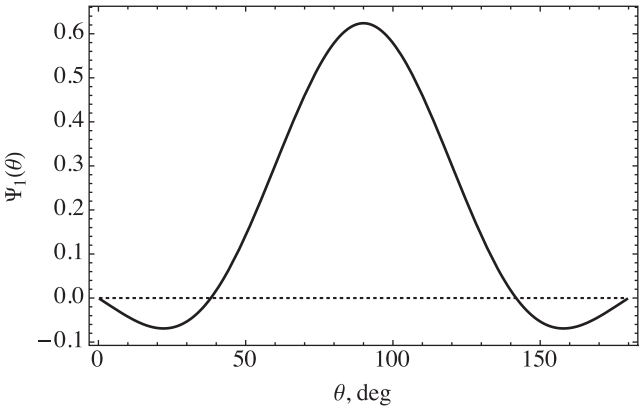

Figure 1. The only solution $\Psi_1(\theta)$ of equation (24), which has no singularity at $\theta = 0$ and $\theta = \pi/2$. The presence of finite solution implies that the disturbance of magnetic flux function decreases as $R_{\rm L}^2/r^2$.

$$B_r = B_{\rm L}\left(\frac{R_{\rm L}}{r}\right)^2\frac{F(\theta)}{\sin\theta}\,{\rm sign}(\cos\theta), \tag{20}$$

$$B_\varphi = E_\theta = -B_{\rm L}\frac{R_s}{r}F(\theta){\rm sign}(\cos\theta), \tag{21}$$

$$B_\theta = E_\varphi = E_r = 0, \tag{22}$$

where $F(\theta) = (4/\pi)\Psi_0'/\Psi_{\rm tot}$, $\Psi_{\rm tot} = \Psi_0(\pi/2)$, and primes indicate the θ-derivatives, e.g. $\Psi_0' = {\rm d}\Psi_0/{\rm d}\theta$. The Michel monopole solution corresponds to $F(\theta) = \sin\theta$. As to equation for the first disturbance $\Psi_1(\theta)$, it looks like

$$\frac{1}{\sin\theta}\frac{\rm d}{{\rm d}\theta}\left(\sin\theta\frac{{\rm d}\Psi_1}{{\rm d}\theta}\right) - \left(\cot^2\theta - 3 + 3\frac{F'}{F}\cot\theta + \frac{F''}{F}\right)\Psi_1 = \Psi_{\rm tot}\frac{1}{\sin\theta}\frac{\rm d}{{\rm d}\theta}\left(\frac{F}{\sin\theta}\right). \tag{23}$$

In particular, for $F(\theta) = \sin\theta$ we obtain $\Psi_1(\theta) = 0$, i.e. pure radial flow. On the other hand, for $\Psi_0'(\theta) = \Psi_{\rm tot}\sin^2\theta$ (and, hence, $B_r \propto \sin\theta$) we obtain

$$\frac{1}{\sin\theta}\frac{\rm d}{{\rm d}\theta}\left(\sin\theta\frac{{\rm d}\Psi_1}{{\rm d}\theta}\right) - \left(9\cot^2\theta - 5\right)\Psi_1 = 2\Psi_{\rm tot}\cot\theta. \tag{24}$$

In Fig. 1 we show the only solution $\Psi_1(\theta)$ of equation (24), which has no singularity at $\theta = 0$ and $\theta = \pi/2$; these two conditions just determine the solution of this equation. As we see, this function is finite and, hence, the disturbance of the radial poloidal magnetic field decreases as $R_{\rm L}^2/r^2$. We will use this property in what follows.

Now, to obtain the fields in the oblique case we use the procedure similar to the one applied in Bogovalov (1999). Instead of multiplying our axisymmetric solution by sign($\cos\theta$) we will multiply it by sign(Φ). As one can easily check, the appropriate fields satisfy Maxwell equations as well except for the current sheet position $\Phi(r, \theta, \varphi) = 0$. Thus, one can conclude that the shape of the current sheet does not depend on the latitudinal structure of the magnetic field.

Finally, using the definitions (20) and (21), one can obtain the following very simple relation between the latitudinal structure of the radial magnetic field $B_r(\theta)$ and the pulsar wind energy flux $S(\theta) = cB_\varphi E_\theta/4\pi$

$$S(\theta) \propto \sin^2\theta\,B_r^2(\theta). \tag{25}$$

The same expression for Poynting flux was also obtained by Tchekhovskoy et al. (2016). For $B_r = $ const. we return to the expression $S(\theta) = \sin^2\theta$, which was widely used in the literature (Bogovalov & Khangoulyan 2002; Komissarov & Lyubarsky 2003). On the other hand, for $B_r(\theta) \propto \sin\theta$ we have

$$S(\theta) \propto \sin^4\theta, \tag{26}$$

i.e. exactly what was obtained numerically by Tchekhovskoy et al. (2013). Of course, as in equation (18), it concerns φ-averaging values. Nevertheless, this result implies that even very simple analytical consideration provides good enough description of the main characteristics of the pulsar wind obtained numerically.

3 CURRENT SHEET IN THE COMOVING REFERENCE FRAME

3.1 MHD approximation

There are two reasons why the force-free model considered above is too simple to describe the main properties of the current sheet. First, in this model the sheet is infinitely thin. Second, within the force-free approximation mass-less particles move with the velocity of light. As one can see from equation (17), the current sheet moves with the same velocity as well, which prevents us from considering its internal structure in detail.

For this reason below, we try to pass to the reference frame comoving with the outflowing plasma. It helps us to separate the intrinsic processes inside the current sheet from the common outflowing motion. Certainly, within the force-free approximation this boost is impossible. For this reason in what follows we use more general MHD approximation formulated in Beskin & Rafikov (2000) (see also Beskin, Zakamska & Sol 2004).

Remember that to describe magnetically dominated MHD outflow it is very convenient to introduce two dimensionless parameters, namely Michel magnetization parameter, $\sigma_{\rm M}$, and multiplicity parameter, λ (Beskin 2010). Here

$$\sigma_{\rm M} = \frac{e\Omega\Psi_{\rm tot}}{8\pi\lambda m_{\rm e}c^3}, \tag{27}$$

where $\Psi_{\rm tot} = \Psi(\pi/2)$ is the total magnetic flux through the upper hemisphere, and

$$\lambda = \frac{n_{\rm e}}{n^0_{\rm GJ}}, \tag{28}$$

where $n^0_{\rm GJ} = \Omega B_{\rm p}/2\pi c|e|$ is the amplitude of the Goldreich–Julian number density. For ordinary pulsars, $\sigma_{\rm M} \sim 10^3$–10^4 and $\lambda \sim 10^3$–10^4, and only for the fast young pulsars (e.g.,Crab, Vela), $\sigma_{\rm M} \sim 10^5$–10^6 and $\lambda \sim 10^4$–10^5. In the force-free limit $m_{\rm e} \to 0$ we have $\sigma_{\rm M} \to \infty$. On the other hand, for finite $\sigma_{\rm M}$ the particle velocity is smaller than that of light (see below). In addition, we suppose that the injection Lorentz factor $\gamma_{\rm in} \sim 10^2$ is constant for all outflowing region.

As a result, according both to the theory (Beskin, Kuznetsova & Rafikov 1998; Prokofev, Arzamasskiy & Beskin 2015) and numerical simulation (Bogovalov & Tsinganos 1999; Bucciantini et al. 2006), the quasi-radial MHD flow is to intersect the fast magnetosonic surface at the distance

$$r_{\rm F} = \min(\sigma_{\rm M}^{1/3}\sin^{-1/3}\theta, \sqrt{\sigma_{\rm M}/\gamma_{\rm in}})\, R_{\rm L}, \tag{29}$$

the Lorentz factor at this surface being

$$\gamma_{\rm F} = \max\left(\sigma_{\rm M}^{1/3}\sin^{2/3}\theta, \gamma_{\rm in}\right). \tag{30}$$

For $\gamma_{\rm in} \gg \sigma_{\rm M}^{1/3}$ (slow rotation) it is necessary to use the second expressions, while for $\gamma_{\rm in} \ll \sigma_{\rm M}^{1/3}$ (fast rotation) they realized in the narrow cone $\theta < \gamma_{\rm in}^{3/2}\sigma_{\rm M}^{-1/2}$ near the rotational axis only; for most angles the first expressions are to be used.

It is very important that for both fast and slow rotations outside the fast magnetosonic surface there are actually no collimation and particle acceleration. More exactly,

$$\gamma \approx \sigma_{\rm M}^{1/3}\sin^{2/3}\theta\log^{1/3}(r/r_{\rm F}) \tag{31}$$

for fast and $\gamma_{\rm F} \approx \gamma_{\rm in}$ for slow rotation (Tomimatsu 1994; Beskin et al. 1998; Prokofev et al. 2015). This implies that with the logarithmic precision one can believe that at large distances $r \gg r_{\rm F}$ the particles move with constant velocity $v_r < c$ exactly corresponding to the drift velocity in $U_{\rm dr}/c = E/B$ (Tchekhovskoy et al. 2009; Beskin 2010). This property just helps us to move into the reference frame comoving with a particular part of the wind (at some constant θ).

3.2 Fields in the comoving reference frame

3.2.1 *Introductory remarks*

As was already stressed, the first attempts in describing the internal structure of the 'striped' pulsar wind were done by Coroniti (1990) and Michel (1994). They based their analysis on magnetic reconnection.

The next step was made by Lyubarsky & Kirk (2001a) describing the internal structure of the moving current sheet by introducing 'fast' and 'slow' variables allowing them to consider the current sheet moving radially with the velocity $v_{\rm sh} < c$. But they did not consider internal structure of a sheet postulating actually zero magnetic field inside it. Later, the following electromagnetic fields were considered (Pétri 2013)

$$B_r(r,\theta,\varphi,t') = B_{\rm L}\frac{R_{\rm L}^2}{r^2}\tanh\left(\frac{R_{\rm L}}{\Delta_{\rm lab}}\Phi_1\right), \tag{32}$$

$$B_\varphi(r,\theta,\varphi,t') = -\frac{B_{\rm L}}{\beta}\frac{R_{\rm L}}{r}\sin\theta\,\tanh\left(\frac{R_{\rm L}}{\Delta_{\rm lab}}\Phi_1\right), \tag{33}$$

$$E_\theta(r,\theta,\varphi,t') == -B_{\rm L}\frac{R_{\rm L}}{r}\sin\theta\,\tanh\left(\frac{R_{\rm L}}{\Delta_{\rm lab}}\Phi_1\right). \tag{34}$$

Here now

$$\Phi_1 = \cos\theta\cos\chi - \sin\theta\sin\chi\cos\left[\varphi - \Omega\left(t' - r/\beta c\right)\right], \tag{35}$$

where t' is the time in the laboratory reference frame, $\beta = v_{\rm sh}/c < 1$ and the function tanh (...) was taken for clear historical reason[2] (this function can be arbitrary).

Unfortunately, these fields cannot be considered as good enough zeroth approximation as they have no force-free limit inside the sheet with finite thickness. Indeed, as can be easily checked, the θ and φ dependencies of the function Φ_1 (35) deny the existence of θ and φ components of the current density inside the sheet even in the force-free approximation. On the other hand, in this limit $j_r = \rho_{\rm e}c$, and, hence, to support the components j_θ and j_φ the particle velocity is to be larger than that of light. By the way, Lyubarsky & Kirk (2001a) did not taken into consideration the radial component of the Maxwell equation $\nabla \times \boldsymbol{B} = \ldots$ (it was postulated that the radial

[2] This function corresponds to well-known Harris (1962) solution.

component of the current density $j_r = 0$ in spite of $[\nabla \times \boldsymbol{B}]_r \neq 0$), so their analysis cannot be considered as self-consistent as well.

Here we present another approach to this problem carrying out calculations in the reference frame moving radially with the current sheet. It allows us to avoid the leading components of electromagnetic fields resulting in the common drift motion. Our consideration is based on the another exact force-free solution obtained by Lyutikov (2011)

$$B_r = B_{\rm L}\left(\frac{R_{\rm L}}{r}\right)^2; \tag{36}$$

$$B_\varphi = E_\theta = -\frac{B_L R_L}{r}\sin\theta\, f(r - ct'), \tag{37}$$

where $f(\dots)$ is again an arbitrary function. Having no dependence on θ and φ, these fields are in agreement with the condition $\boldsymbol{j} = \rho_{\rm e} c\,\mathbf{e}_r$. We can use this solution for inclined rotator because the shape of the current sheet in this case is similar to the spherical wave (see, e.g. Kalapotharakos et al. 2012).

Of course, it is necessary to stress that this solution contains no sign change of the radial component of the magnetic field B_r. On the other hand, as already mentioned above, outside the fast magnetosonic surface $r \gg r_{\rm F} \sim \sigma_{\rm M}^{1/3} R_{\rm L}$ (29) both the disturbance of the monopole poloidal magnetic field resulting from the MHD disturbances (Beskin et al. 1998) and the disturbances (19) connecting with θ-dependence of the poloidal field have the same smallness $\sim\sigma_{\rm M}^{-2/3}$ at the fast surface and, hence, can be neglected.

For this reason, in what follows we put $B_r = 0$. As is well known, this approximation is good enough outside the fast magnetosonic surface $r > r_{\rm F}$ and widely used in analysis of the pulsar wind (Lyubarsky & Kirk 2001a; Brennan & Gralla 2014). Indeed, according to equations (29)–(30), for fast rotator in the comoving reference frame the toroidal magnetic field $B'_\varphi = B_\varphi/\gamma$ becomes larger than poloidal one $B'_r = B_r$ just outside the fast surface; for slow rotator it takes place even at smaller distances.

As a result, we can modify now this solution for arbitrary θ-dependence of the poloidal magnetic field $B_{\rm r}(\theta)$, which, as was already stressed, better corresponds to the real structure of the pulsar wind. For $f \equiv -\tanh$ the fields in the laboratory frame (r, θ, φ, t') can be presented as

$$B_\varphi(r,\theta,t') = \frac{1}{\beta}\frac{B_L R_L}{r}F(\theta)\tanh\left(\frac{r-\beta ct'}{\Delta_{\rm lab}}\right), \tag{38}$$

$$E_\theta(r,\theta,t') = \frac{B_L R_L}{r}F(\theta)\tanh\left(\frac{r-\beta ct'}{\Delta_{\rm lab}}\right), \tag{39}$$

where $\Delta_{\rm lab}$ is a current sheet thickness in the laboratory reference frame, and $F(\theta)$ now is the arbitrary function. As was already stressed, the parameter $\beta = E_\theta/B_\varphi$ can be considered here as a constant.

Accordingly, the charge density in this frame is equal to Goldreich–Julian charge density:

$$\rho_{\rm e} = -\frac{B_L R_L}{4\pi r^2\sin\theta}\frac{{\rm d}[F(\theta)\sin\theta]}{{\rm d}\theta}\tanh\left(\frac{r-\beta ct'}{\Delta_{\rm lab}}\right) = n_{GJ} e, \tag{40}$$

but the current density is now equal to

$$j = \frac{\rho_{\rm e}}{\beta}. \tag{41}$$

This implies that within the MHD approximation the velocities of electron and positron components are to be different. In magnetically dominated case, one can seek the first-order corrections in the following form:

$$v_r^\pm/c = 1 - \xi_r^\pm;\ v_\theta^\pm/c = \xi_\theta^\pm;\ v_\varphi^\pm/c = \xi_\varphi^\pm. \tag{42}$$

As the particle number densities can be now written as

$$n^\pm = n_{\rm GJ}\left[\lambda \mp \frac{1}{4}\hat{D}_\theta F(\theta)\right], \tag{43}$$

where $\hat{D}_\theta F(\theta) = F'(\theta) + F(\theta)\cot\theta$ (e.g. $\hat{D}_\theta \sin\theta = 2\cos\theta$), one can obtain using the definition of the current density $j = en^+ v_r^+ - en^- v_r^-$

$$\xi_r^\pm = 1 - \beta \pm \frac{1}{2\lambda\gamma^2\beta}, \tag{44}$$

or

$$v_r^\pm/c = \beta \mp \frac{1}{2\lambda\gamma^2\beta}. \tag{45}$$

Here $\gamma = (1 - v^2/c^2)^{-1/2}$ is the Lorentz factor and λ again is the multiplicity parameter.

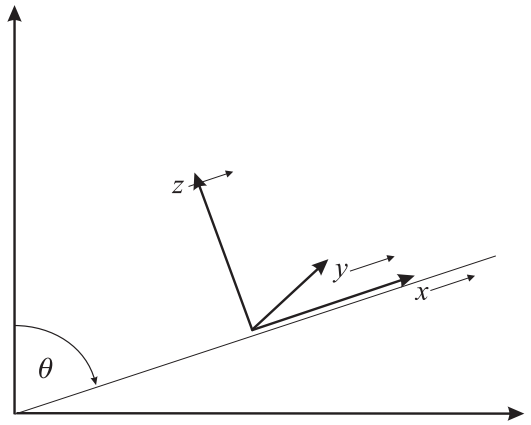

Figure 2. Inertial reference frame (x, y, z, t) moving radially with velocity $V = \beta c$.

3.2.2 *Comoving reference frame – orthogonal case*

As was already stressed, important property of the solutions (38)–(39) presented above is that the parameter β can be considered as a constant. Thus, the reference frame moving radially with the velocity $V = \beta c$ is the inertial one. In order to study the field structure in this reference frame moving with the current sheet, we need to express the fields in Cartesian coordinates and make a Lorentz transform:

$$B'_x = B_x;\ B'_y = \Gamma(B_y + \beta E_z);\ B'_z = \Gamma(B_z - \beta E_y), \tag{46}$$

$$E'_x = E_x;\ E'_y = \Gamma(E_y - \beta B_z);\ E'_z = \Gamma(E_z + \beta B_y). \tag{47}$$

Here and below $\Gamma = (1 - \beta^2)^{-1/2}$ is the boost Lorentz factor, and the values without prime correspond to the reference frame moving radially with the x-axis directed along the radius vector $\mathbf{e}_r$ and the y-axis along $\mathbf{e}_\varphi$ (see Fig. 2). As a result, near the origin of the reference frame moving radially with the velocity $V = \beta c$ (and for $f \equiv -\tanh$) the first-order fields look like

$$B_y(x,y,z,t) = B_0\frac{R_{\rm L}}{ct}\left(1 - \frac{z^2}{c^2 t^2}\right)\tanh\left(\frac{x}{\Gamma\Delta_{\rm lab}}\right), \tag{48}$$

$$E_x(x, y, z, t) = B_0 \frac{R_L z}{c^2 t^2} \tanh\left(\frac{x}{\Gamma \Delta_{lab}}\right). \quad (49)$$

Here $x = \Gamma(r - \beta c t')$, $t = t'/\Gamma$ is the time in the comoving reference frame, and

$$B_0 = \frac{B_L}{\beta^2 \Gamma^2} F(\theta), \quad (50)$$

which now can be considered as a constant. Note that this expression has Γ^2 instead of Γ in denominator since B_0 actually represents magnetic field at fast magnetosonic surface in comoving frame. Fast magnetosonic surface corresponds to the time $t'_0 = r_F/\beta c \Rightarrow t_0 \approx R_L/c$. Finally, as $z \ll ct$, we do not include the factor below $(1 - z^2/c^2t^2)$ into consideration.

Further, as one can directly check, Maxwell equation $c\nabla \times \boldsymbol{E} = -\partial \boldsymbol{B}/\partial t$ is automatically fulfilled. Finally, for another Maxwell equation $c\nabla \times \boldsymbol{B} = \partial \boldsymbol{E}/\partial t + 4\pi \boldsymbol{j}$ to be valid, two-fluid MHD consideration is necessary. This question will be considered in detail in Section 4. At this moment we only stress that the charge density along the boost axis (i.e. x-axis) is equal to 0, and the particle velocities after the Lorentz transform become

$$\frac{v_x^{\pm}}{c} = \mp \frac{1}{(2\lambda \pm 1)\beta} \approx \mp \frac{1}{2\lambda\beta}. \quad (51)$$

Expressions (48)–(49) are our main intermediate result giving zero approximation for the internal structure of the quasi-spherical current sheet in its comoving reference frame. As we see, this solution is essentially time dependent. Indeed, r^{-1} diminishing of the toroidal magnetic field B_φ in the pulsar wind transforms into t^{-1} time dependence in the comoving reference frame. As will be shown below, this results in a set of new effects which does not exist in classical time-independent configurations.

3.2.3 *Comoving reference frame – aligned case*

Similarly, one can consider the internal structure of the current sheet for the axisymmetric case when the current sheet locates in the equatorial plane. After passing into comoving reference frame (the calculations are quite similar to Section 3.2.2) we obtain for the leading components of electromagnetic field ($\theta = \pi/2$):

$$B_y(x, y, z, t) = B_0 \frac{R_L}{ct} \tanh\left(\frac{z}{\Gamma \Delta_{lab}}\right), \quad (52)$$

$$E_x(x, y, z, t) = B_0 \frac{R_L z}{c^2 t^2} \tanh\left(\frac{z}{\Gamma \Delta_{lab}}\right). \quad (53)$$

These fields differ from equations (48)–(49) by z (not x) coordinate perpendicular to the sheet plane.

It is necessary to stress that recent PIC simulations of the axisymmetric pulsar magnetosphere (Cerutti et al. 2015) demonstrate non-stationarity of the equatorial sheet so that a high-amplitude wave is generated just outside the light cylinder. In other words, axisymmetric equatorial sheet actually cannot exist. Nevertheless, we consider this case as well.

4 INTERNAL STRUCTURE OF TIME-DEPENDENT CURRENT SHEET

In this section, we discuss in detail the structure of electromagnetic fields and particle drift motion for time-dependent current sheet not far from the fast magnetosonic surface. In this domain the time-dependent effects are most pronounced. Most of this section is devoted to discussion of orthogonal case, while aligned case is discussed in the appendix.

In our analysis, we do not consider the important effects related to different instabilities (e.g. tearing and drift-kink) which can drastically disturb the structure of a sheet. The inclusion of these effects is beyond the scope of this study and we leave it for the following paper.

Note that, for simplicity we use $f(x) = \tanh(x)$ form of the current sheet (Harris sheet), everywhere except for Section 4.1. The results can be easily applied to any physically reasonable form, i.e. odd function with

$$\lim_{x \to \pm\infty} f(x) \to \pm 1$$

and $f(0) = 0$.

4.1 Accelerating electric field

As was already stressed, solutions (48)–(49) constructed above correspond to the constant width Δ_{lab} of the current sheet separating time-dependent magnetic fluxes. To describe the time evolution of the current sheet width $\Delta_{lab}(t)$ (which is one of the main goals of this paper), it is necessary to include into accelerating another component of the electric field, E_z.

To show this, it is convenient to rewrite the relations (48)–(49) in the form

$$B_y(x, y, z, t) = B_0 \frac{R_L}{ct} h(x, t), \quad (54)$$

$$E_x(x, y, z, t) = B_0 \frac{R_L z}{c^2 t^2} h(x, t), \quad (55)$$

where $h(x, t) = f[x/\Delta(t)]$. Then, we can rewrite Maxwell equation $c\nabla \times \boldsymbol{E} = -\partial \boldsymbol{B}/\partial t$ as

$$\frac{\partial E_z}{\partial x} = B_0 \frac{R_L}{c^2 t} \frac{\partial h}{\partial t}. \quad (56)$$

It gives

$$E_z = B_0 \frac{R_L}{c^2 t} \frac{\partial}{\partial t} \left(\int_{\infty}^{x} h(x', t) \mathrm{d}x' \right). \quad (57)$$

Further, as $f(x)$ and $h(x, t)$ are both odd functions of x, one can choose the integrating constant for $E_z \propto \int h(x', t)\mathrm{d}x'$ to be even function with clear boundary conditions $E_z(\pm\infty) = 0$. Clearly, in this case we obtain $E_z(x = 0) \neq 0$ near the centre plane of the current sheet. Finally, Maxwell equation $c\nabla \times \boldsymbol{B} = \partial \boldsymbol{E}/\partial t + 4\pi \boldsymbol{j}$ now looks like

$$B_0 \frac{R_L}{ct} \frac{\partial h}{\partial x} = \frac{1}{c} \frac{\partial E_z}{\partial t} + \frac{4\pi}{c} j_z. \quad (58)$$

For Harris current sheet one can obtain the following expressions:

$$B_y = B_0 \frac{t_0}{t} \tanh \frac{x}{\Delta(t)}, \quad (59)$$

$$E_x = B_0 \frac{t_0 z}{ct^2} \tanh \frac{x}{\Delta(t)}, \quad (60)$$

$$E_z = B_0 \frac{t_0 \Delta'(t)}{ct} \left\{ \log\left[2 \cosh \frac{x}{\Delta(t)}\right] - \frac{x}{\Delta(t)} \tanh \frac{x}{\Delta(t)} \right\}. \quad (61)$$

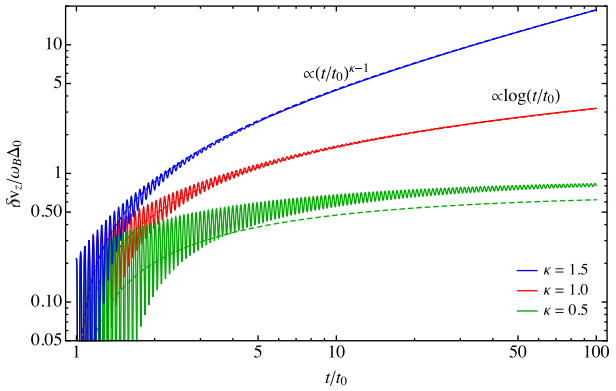

Figure 3. The acceleration of particles along the sheet by an additional electric field for different expansion parameters κ. Solid lines correspond to the time dependence of particle velocity, and dashed lines represent analytical prediction (63).

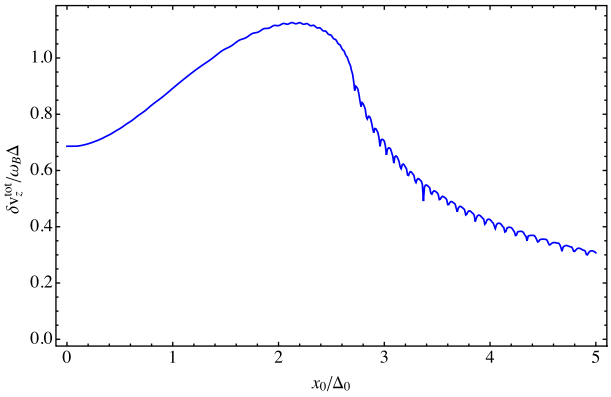

Figure 4. Dependence of the total acceleration in the sheet with $\kappa = 0.5$ on the initial coordinate of the particle. Acceleration increases until $x_0/\Delta_0 \sim 2.5$. It corresponds to the last initially trapped orbit. Particles with larger x_0 move outside the sheet until getting trapped, and the total change in velocity decreases.

As we see, time dependence of the current sheet thickness $\Delta(t)$ inevitably results in the appearance of the non-zero electric field E_z along the sheet which is larger than the magnetic one near the zero surface. Thus, the evolution of the current sheet width and the problem of particle acceleration cannot be considered separately.

Acceleration of particles could be estimated by considering particles trapped deep inside the current sheet $x \ll \Delta$. For such particles, the change of z-component of momentum due to E_z could be found from the solution of

$$\dot{p}_z \approx eB_0 \frac{t_0\Delta'(t)}{ct}\log(2), \tag{62}$$

giving the acceleration

$$\delta p_z(t) = \int_{t_0}^{t} \dot{p}_z \mathrm{d}t = \frac{\kappa\log(2)}{\kappa-1}\frac{eB_0\Delta_0}{c}[(t/t_0)^{\kappa-1} - 1]. \tag{63}$$

Here $\Delta'(t) = \mathrm{d}\Delta/\mathrm{d}t$, and we assume power-law dependence for the current sheet thickness $\Delta(t) \propto t^{\kappa}$. Equation (63) is valid for $\kappa \neq 1$. For $\kappa = 1$, integration (63) gives logarithmic divergence. For such case we assume $\delta p_z \approx eB_0\Delta_0/c = \text{const}$. For $\kappa < 1$, δp_z asymptotically goes to constant. In this case we also set $\delta p_z \approx eB_0\Delta_0/c = \text{const}$. On the other hand, for $\kappa > 1$ momentum grows as $t^{\kappa-1}$ with time. Combining all the expressions, one can approximate the acceleration of particles in the current sheet as

$$\delta p_z(t) = eB_0\Delta_0/c, \qquad \kappa \leq 1 \tag{64}$$

$$\delta p_z(t) = eB(t)\Delta(t)/c, \qquad \kappa > 1 \tag{65}$$

where $B(t)$ is the value of magnetic field outside of the current sheet $B(t) = B_0(t_0/t)$.

In Fig. 3, expression (63) is compared with the exact solution of particle equations of motion in fields (59)–(61) for different κ. The numerical solution is in good agreement with analytical prediction, except for $\kappa = 0.5$. The small difference between analytical and numerical solution in $\kappa = 0.5$ case is examined in Fig. 4. All particles examined for this figure start with $z_0 = 0$, $v_x = 0$, $v_z = \omega_B\Delta_0$ and with different initial x_0. An analytical value $\delta v_z = \log 2\omega_B\Delta_0$ corresponds to the limit of this curve at $x_0 \to 0$. For larger x_0, acceleration is larger, but order of magnitude remains the same. We thus conclude that estimations (64)–(65) are in good agreement with numerical solution.

4.2 Particle drift outside the current sheet

In this section, we discuss the main manifestations of time-dependent effects in the proper reference frame of the current sheet. First of all, in the comoving reference frame the particles experience drift motion outside the current sheet ($x \gg \Delta$ for orthogonal case and $z \gg \Delta$ for aligned case). The fastest component of such motion is the z component of electric drift

$$U_z = c\frac{E_x B_y}{B_y^2} = \frac{z}{t}. \tag{66}$$

This velocity exactly corresponds to the radial divergence of the flow due to radial expansion. Since within our approximation $z \ll ct$, the drift velocity of particles remains non-relativistic.

The drift velocity U_z is directed along the current sheet in orthogonal case, and out of the sheet in aligned case. In orthogonal case it implies that the particle, which is outside of the current sheet initially, will move along the sheet until its orbit starts to intersect the midplane of the sheet. After this moment the particle is trapped and no longer drifts. On the other hand, in aligned case, particles drift away from the sheet. If current sheet expands slowly enough, such particles will never get trapped. Similarly, the particles, which are initially trapped might escape the sheet and start to drift with velocity $U_{\rm esc}^{\rm align} = \Delta(t_{\rm esc})/t_{\rm esc}$, where $t_{\rm esc}$ is the time when particle escapes the sheet. One can easily find that escape can only occur if $\Delta(t)$ expands slower than linear.

As shown in Section 4.1, in orthogonal case the additional time dependence of a sheet width leads to additional electric field diminishing exponentially outside the sheet: $E_{\rm add} \propto \exp(-x/\Delta)$. Since for particles outside the sheet $\Delta \ll x$, we can neglect this electric field. The same remains true for gradient drift.

Further, Larmor radius of particles changes due to the conservation of the first adiabatic invariant $p_\perp^2/B_y \approx \text{const}$. This connection allows us to evaluate the dependence of gyroradius on time (cf. Lyubarsky & Kirk 2001a)

$$\mathcal{R}_{\rm L}(t) = \mathcal{R}_{\rm L}(t_0)\left(\frac{t}{t_0}\right)^{1/2}. \tag{67}$$

Such a dependence shows that the gradient drift (or any other drifts except electric) is not just significantly smaller than z component of

electric drift, but also smaller compared to Larmor radius growth. For orthogonal case equations (66) and (67) indicate that any particle that initially is outside the sheet eventually gets trapped inside the sheet.

Now we can compare an average gyroradius of particles with the thickness of sheet. If gyroradius of a particle is much smaller than the width of the current sheet, it is possible to use the drift approximation. The only component of the drift velocity having x component is the electric drift $U_x = -cE_zB_y/B^2$

$$U_x = -\Delta'(t)\left\{\frac{\log\left[2\cosh(x/\Delta)\right]}{\tanh(x/\Delta)} - x/\Delta\right\}, \tag{68}$$

In particular, for $x \ll \Delta_0$ we have

$$U_x = -\log(2)\frac{\Delta'(t)\Delta(t)}{x}. \tag{69}$$

Certainly, it is impossible to use this evaluation in the very centre of a sheet $x \to 0$ where $E_z > B_y$.

As one can see, for $\Delta \gg \mathcal{R}_\mathrm{L}$, when there are a lot of particles with $\mathcal{R}_\mathrm{L} \ll |x| < \Delta$, which do not cross the null surface, these particles will drift towards $x = 0$. This results in slow collapse of the sheet until the current sheet becomes thin enough so $\mathcal{R}_\mathrm{L} \sim \Delta$.

On the other hand, it is impossible to sustain the Harris current sheet if $\mathcal{R}_L \gg \Delta$ as the particles in such a sheet spend most of their time in the region $|x| > \Delta$, i.e. outside of the sheet. This leads to the conclusion that in realistic current sheet $\mathcal{R}_\mathrm{L} \sim \Delta$.

Finally, time dependence of the current sheet results in the trapping of particles in the vicinity of the null surface. We illustrate this effect in Fig. 5 where we show the trajectories of drifting particles outside the sheet. All particles start with the same velocity and x_0, but with different z_0. Points correspond to the positions of particles at the same moment in time showing that the time required for particle to get trapped is almost independent of z_0, and is determined by the x component of drift velocity (68).

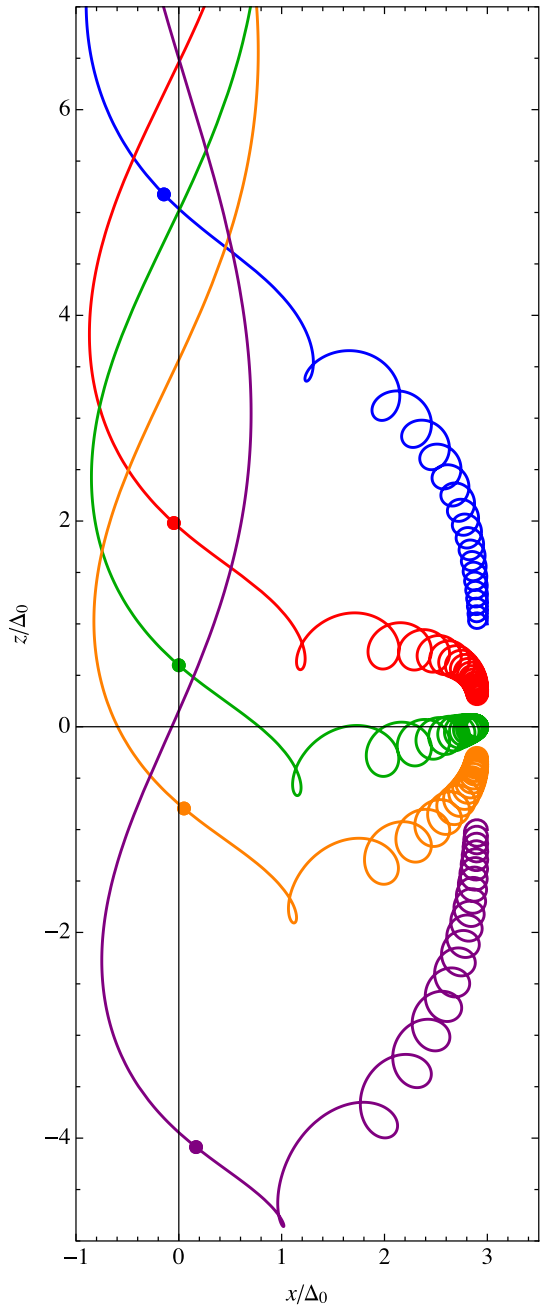

Figure 5. Trapping of particles in the orthogonal current sheet for different starting positions outside the sheet. The points correspond to the positions of particles at the same moment in time. As x-positions of these points are close, the time until particles get trapped is the same for particles with the same initial x.

4.3 Self-consistent solutions for non-relativistic particles

In this section, we find exact solution for a particle trapped deep inside the orthogonal current sheet $x \ll \Delta$. Surprisingly, the equations for non-relativistic particles could be integrated exactly. For relativistic particles not only equations could not be solved analytically, but also the actual approximation $x, z \ll ct$ breaks down and the fields (59)–(61) could not be used.

In the orthogonal case, we can use expressions (59)–(61) for electromagnetic fields:

$$B_y = B_0\frac{t_0}{t}\tanh\frac{x}{\Delta(t)}, \tag{70}$$

$$E_x = B_0\frac{t_0 z}{ct^2}\tanh\frac{x}{\Delta(t)} \tag{71}$$

$$E_z = \kappa\frac{B_0 t_0\Delta(t)}{ct^2}\left\{\log\left[2\cosh\frac{x}{\Delta(t)}\right] - \right. \tag{72}$$

$$\left.\frac{x}{\Delta(t)}\tanh\frac{x}{\Delta(t)}\right\}, \tag{73}$$

where we again assume $\Delta(t) \propto t^\kappa$. After substitution of these expressions into equation of motion we obtain the following system of equations:

$$\ddot{z} = \frac{eB_0t_0}{m_\mathrm{e}ct}\left\{\dot{x}\tanh\frac{x}{\Delta(t)} + \right. \tag{74}$$

$$\left. + \kappa\frac{\Delta(t)}{t}\log\left[2\cosh\frac{x}{\Delta(t)}\right] - \kappa\frac{x}{t}\tanh\frac{x}{\Delta(t)}\right\},$$

$$\ddot{x} = \frac{eB_0t_0}{m_\mathrm{e}ct^2}\tanh\frac{x}{\Delta(t)}(z - \dot{z}t). \tag{75}$$

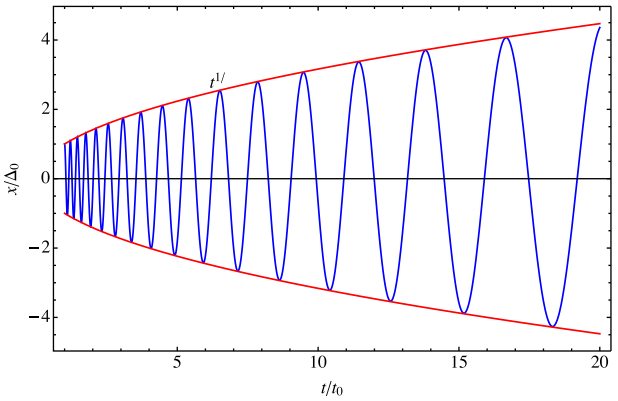

Figure 6. Comparison of numerical solution for motion of particle inside the sheet (blue oscillating line) with analytical prediction (82). Red asymptotic line shows the dependence of amplitude of particle oscillations on time $x_{\max} = x_0 t^{1/2}/t_0^{1/2}$.

Integrating the first equation now, one can obtain

$$z - \dot{z}t = -\Delta(t)\Lambda \log\left[2\cosh\frac{x}{\Delta(t)}\right] + C \tag{76}$$

corresponding to conversation of the following invariant

$$I = m_e z - P_z t. \tag{77}$$

Here $\Lambda = \omega_B t_0$ ($\omega_B = eB_0/m_e c$ is cyclotron frequency), and $P_z = p_z + eA_z$ is generalized momentum. This integral remains constant for non-relativistic case only. Further, substituting equation (76) into equation (75) we obtain

$$\ddot{x} = -\Lambda^2 \frac{\Delta(t)}{t^2}\tanh\frac{x}{\Delta(t)}\log\left[2\cosh\frac{x}{\Delta(t)}\right]. \tag{78}$$

Here we neglect the constant C in comparison with $\Delta(t)$ which is possible for expanding sheet.

To evaluate the asymptotic behaviour of non-linear equation (78) (which has no exact analytical solution) we present the coordinate $x(t)$ in the form $x(t) = \Delta(t)S(t)$ where $S(t)$ is a restricted function. After substituting this into equation (78) we obtain

$$t^2 S'' + 2\kappa t S' + \kappa(\kappa - 1)S = -\Lambda^2 \tanh S \log[2\cosh S], \tag{79}$$

where primes indicate derivatives over t.

Expanding now RHS into Maclaurin series (which is possible for $S \ll 1$) we obtain for the leading term

$$t^2 S'' + 2\kappa t S' + \log(2)\Lambda^2 S = 0. \tag{80}$$

Here we suppose that $\Lambda \simeq 4\lambda\sigma_M \gg 1$. Equation (80) is linear and have the following solutions

$$S_\pm = S_0\, t^{-(2\kappa-1)/2}\cos\left[\sqrt{\log(2)}\Lambda\log(t) + \varphi_\pm\right]. \tag{81}$$

As a result, it becomes clear that unless $\kappa \neq 1/2$ the expansion of the sheet doesn't follow the expansion of particle trajectory, for which we have

$$x(t) \approx x_0\left(\frac{t}{t_0}\right)^{1/2}\cos\left[\alpha(x_0)\Lambda\log(t) + \varphi_0\right] \tag{82}$$

for arbitrary oscillation amplitude x_0. The constant $\alpha(x_0)$ slowly varies between $\sqrt{\log(2)}$ at $x_0 \ll \Delta$ and unity for $x_0 \gg \Delta$. An analytical solution (82) is compared with numerical solution in Fig. 6 demonstrating their good agreement. It is also clear from equation (81) that the growth rate proportional to square root of time is a solution for arbitrarily expanding sheet.

4.4 Current sheet thickness and particle acceleration

In the previous section, we have found self-consistent solution for internal structure of current sheet; however, in this section we will show that such solution cannot be asymptotic one. Below we evaluate the current sheet thickness based on its global structure. We will explore MHD equations in order to find asymptotic behaviour of current sheet.

Starting from Faraday's law

$$\frac{B}{\Delta} = 8\pi n_{\rm in} e\frac{v_z}{c} \tag{83}$$

and combining it with the definition of multiplicity λ, we can express thickness of the current sheet through $v_z(t)/c$ and $n_{\rm out}/n_{\rm in}$ parameters:

$$\Delta = R_L \frac{t}{t_0}\frac{\Gamma}{4\lambda}\frac{c}{v_z}\frac{n_{\rm out}}{n_{\rm in}}. \tag{84}$$

Here $n_{\rm out}$ and $n_{\rm in}$ refer to particle number density outside and inside the current sheet, respectively.

It is clear that asymptotically v_z/c grows up to a constant value. For $v_z(\infty)/c < 1$ we get non-relativistic case, which correspond to particle motion discussed above. It is possible to determine value of $\delta p_z \simeq eB\Delta/c$:

$$\delta p_z = m_e c\Gamma^2 \frac{c}{v_z}\frac{n_{\rm out}}{n_{\rm in}}. \tag{85}$$

This expression could be used for $\kappa \geq 1$ to get $\delta p_z(t)$, or for $\kappa < 1$ to get $\delta p_z(\infty)$. In the latter case, the values of v_z, $n_{\rm in}$ and $n_{\rm out}$ should be taken at $t = t_0$.

From equation (85) one can see that if the sheet is relativistic ($v_z \sim c$) and $n_{\rm in} \sim n_{\rm out}$, the particle can reach a Lorentz factor $\gamma_e \sim \Gamma^2 = \sigma_M^{2/3}$. It is obvious that such rapid acceleration breaks some of the assumption made in the beginning (e.g. the Lorentz factor of the current sheet in the laboratory frame is only Γ). On the other hand, one may expect that in realistic sheet $n_{\rm in} \gg n_{\rm out}$, so $\gamma_e \ll \Gamma^2$.

Further, as shown earlier, the sheet with $\Delta \gg \mathcal{R}_L$ collapses. Under this condition the force balance perpendicular to the sheet plane can be written as

$$\frac{B^2}{8\pi} = n_{\rm in}\mathcal{E}_k, \tag{86}$$

where $\mathcal{E}_k(t)$ is the particle thermal kinetic energy inside the sheet. Using now the definition (27) for magnetization parameter σ_M, one can rewrite this relation in a simple form

$$\frac{\mathcal{E}_k}{m_e c^2} = \frac{\sigma_M}{\Gamma}\frac{n_{\rm out}}{n_{\rm in}}. \tag{87}$$

As we see, non-relativistic approximation inside the sheet is valid for high enough number density

$$\frac{n_{\rm in}}{n_{\rm out}} > \sigma_M^{2/3}. \tag{88}$$

As a result, comparing relations (84) and (87) one can conclude that linear increase of the sheet thickness $\Delta \propto t$ predicted by Coroniti (1990) and Michel (1994) and recently reproduced in numerical simulation (Philippov, Spitkovsky & Cerutti 2015) can be realized for constant particle energy $\mathcal{E}_k$ and constant ratio $n_{\rm in}/n_{\rm out}$ only. The first condition $\mathcal{E}_k \approx$ const. is in agreement with time-independent acceleration energy along the sheet. On the other hand, the second one $n_{\rm in}/n_{\rm out} \approx$ const. can be realized only if the particle inflow significantly increases the number of particles inside the sheet. Such

an inflow was also reproduced in numerical simulations (see e.g. Cerutti et al. 2015).

Besides, if the plasma is hot, $\mathcal{E}_k > m_e c^2$, we obtain for the Larmor radius

$$\langle \mathcal{R}_L \rangle = \frac{c\langle p_\perp \rangle}{eB} = \frac{\mathcal{E}_k}{eB} = R_L \frac{t}{t_0} \frac{\Gamma}{4\lambda} \frac{n_{out}}{n_{in}}. \quad (89)$$

As one can see, $\langle \mathcal{R}_L \rangle = \Delta \cdot v_z/c$. Thus, for the condition $\Delta \sim \mathcal{R}_L$ to be fulfilled, relativistically hot current sheet requires $v_z \sim c$.

On the other hand, if the number density outside the sheet is much smaller than inside, the number of particles inside the sheet cannot increase. This will lead to $n_{in} \propto t^{-3}$, but n_{out} will be proportional to t^{-2}. So the ratio between n_{out} and n_{in} should be of order unity. In this case particle acceleration can be estimated as

$$\delta p_z \simeq m_e c \Gamma^2, \quad (90)$$

or, in laboratory frame,

$$\delta p_z^{lab} \simeq m_e c \Gamma, \quad (91)$$

which is of the same order as mean thermal momentum of particles inside current sheet.

5 DISCUSSION AND CONCLUSIONS

This paper provides the formalism to describe essentially time-dependent evolution of the current sheet in the pulsar wind. As the first step in this direction, we carry out the calculations in the co-moving reference frame and successfully determine intrinsic electromagnetic fields of the current sheet. In our opinion, this approach allows us to describe the physical processes in a sheet more vividly.

In the first part of this paper we investigate asymptotic structure of the wind from rotating oblique neutron star using force-free approximation. General asymptotic solution of the Grad–Shafranov equation for quasi-spherical pulsar wind up to the second order in small parameter $\varepsilon = (\Omega r/c)^{-1}$ was obtained. We have shown that the wind can have arbitrary latitude dependence on the energy flux. In particular, our solution describes the latitudinal structure of the radial magnetic field obtained numerically for oblique rotator. The form of current sheet in asymptotic does not depends on its latitudinal structure and matches the one in Bogovalov solution (Bogovalov 1999).

As the force-free approximation does not allow us to discuss the inner structure of the current sheet, we use MHD approximation in which the velocity of the pulsar wind is assumed to be less than that of light. Indeed, as is well known (see, e.g. Beskin et al. 1998), outside the fast magnetosonic surface the velocity of quasi-spherical MHD flow becomes almost constant. Using this property (and carrying out calculations in the comoving reference frame), we estimate the efficiency of the particle acceleration inside the sheet.

The main conclusion of our consideration is that the intrinsic time dependence of a sheet in the comoving reference frame (especially the increase of the sheet thickness Δ) inevitably results in the appearance of the electric field which is larger than the magnetic one inside the sheet. It is this electric field that controls the electric current of a sheet.

Finally, after investigating the motion of individual particles in the time-dependent current sheet, we evaluate the width of the sheet and its time evolution. In particular, we considered both relativistic and non-relativistic temperatures inside the sheet.

In particular, it was shown that while the individual particle orbit grows as $t^{1/2}$, the sheet as a whole should grow linearly with time. This contradiction can be solved by using methods of kinetic equation. Since the particle flow inside a sheet due to its expansion is considerable, the evolution of current sheet can be defined by incoming particles and not by the evolution of individual particles inside the sheet.

As for particle acceleration, it was shown that in relativistic case when number density inside the sheet is similar to one outside the sheet, particle gains additional $m_e c \sigma^{1/3}$ momentum (in laboratory frame) due to expansion of a sheet. It is important to notice that although the acceleration region $|\boldsymbol{E}| > |\boldsymbol{B}|$ is narrow, the trajectories of particles are adjusted in such a way that they accelerate in the MHD region $|\boldsymbol{E}| < |\mathbf{B}|$ every half period in one direction, cross the $|\mathbf{E}| > |\boldsymbol{B}|$ zone and then accelerate in the same direction again (see Fig. 5).

Finally, it is important to highlight the difference between this paper and Lyubarsky & Kirk (2001b) in which authors use global equation in order to determine growth of current sheet thickness. In our work we do not consider reconnection, so our result should be interpreted as pre-reconnection sheet structure. However, the electric field, which results from time dependence of sheet thickness in the case of linear growth, has the same structure as reconnection field and it is possible, that even in the case of reconnection, our description of individual particle motion remains relevant.

ACKNOWLEDGEMENTS

We thank Ya.N. Istomin and A.Philippov for their interest and useful discussion and the anonymous referee for instructive comments which helped us to improve the manuscript. This research was partially supported by the government of the Russian Federation (agreement No. 05.Y09.21.0018) and by Russian Foundation for Basic Research (Grant no. 15-02-03063).

REFERENCES

Aharonian F. et al., 2007, A&A, 464, 235
Aharonian F. A., Bogovalov S. V., Khangulyan D., 2012, Nature, 482, 507
Arons J., 1981, ApJ, 248, 1099
Arons J., 2012, Space Sci. Rev., 173, 341
Beskin V. S., 2010, MHD Flows in Compact Astrophysical Objects. Springer-Verlag, Berlin
Beskin V. S., Rafikov R. R., 2000, MNRAS, 313, 433
Beskin V. S., Gurevich A. V., Istomin Y. N., 1993, Physics of the Pulsar Magnetosphere. Cambridge Univ. Press, Cambridge
Beskin V. S., Kuznetsova I. V., Rafikov R. R., 1998, MNRAS, 299, 341
Beskin V. S., Zakamska N. L., Sol H., 2004, MNRAS, 347, 587
Blandford R. D., 1975, MNRAS, 170, 551
Bogovalov S. V., 1999, A&A, 349, 1017
Bogovalov S. V., Khangoulyan D. V., 2002, Astron. Lett., 28, 373
Bogovalov S., Tsinganos K., 1999, MNRAS, 305, 211
Brennan T. D., Gralla S. E., 2014, Phys. Rev. D, 89, 103013
Bucciantini N., Thompson T. A., Arons J., Quataert E., Del Zanna L., 2006, MNRAS, 368, 1717
Cerutti B., Philippov A., Parfrey K., Spitkovsky A., 2015, MNRAS, 448, 606
Contopoulos I., Kazanas D., Fendt C., 1999, ApJ, 511, 351
Contopoulos I., Kalapotharakos C., Kazanas D., 2014, ApJ, 781, 46
Coroniti F. V., 1990, ApJ, 349, 538
Gruzinov A., 2005, Phys. Rev. Lett., 94, 021101
Harris E., 1962, Il Nuovo Cimento, 23, 115
Ingraham R. L., 1973, ApJ, 186, 625
Kalapotharakos C., Contopoulos I., Kazanas D., 2012, MNRAS, 420, 2793

Komissarov S. S., 2006, MNRAS, 367, 19
Komissarov S. S., Lyubarsky Y. E., 2003, MNRAS, 344, L93
Levinson A., 2000, Phys. Rev. Lett., 85, 912
Lyubarsky Y., Kirk J. G., 2001a, ApJ, 547, 437
Lyubarsky Y. E., Kirk J. G., 2001b, PASA, 18, 415
Lyutikov M., 2011, Phys. Rev. D, 83, 124035
Mestel L., 1973, Ap&SS, 24, 289
Michel F. C., 1973, ApJ, 180, L133
Michel F. C., 1994, ApJ, 431, 397
Okamoto I., 1974, MNRAS, 167, 457
Pétri J., 2013, MNRAS, 434, 2636
Philippov A. A., Spitkovsky A., Cerutti B., 2015, ApJ, 801, L19
Prokofev V. V., Arzamasskiy L. I., Beskin V. S., 2015, MNRAS, 454, 2146
Ruderman M. A., Sutherland P. G., 1975, ApJ, 196, 51
Spitkovsky A., 2006, ApJ, 648, L51
Sturrock P. A., 1971, ApJ, 164, 529
Tchekhovskoy A., McKinney J. C., Narayan R., 2009, ApJ, 699, 1789
Tchekhovskoy A., Spitkovsky A., Li J. G., 2013, MNRAS, 435, L1
Tchekhovskoy A., Philippov A., Spitkovsky A., 2016, MNRAS, 457, 3384
Timokhin A. N., 2006, MNRAS, 368, 1055
Timokhin A. N., Arons J., 2013, MNRAS, 429, 20
Tomimatsu A., 1994, PASJ, 46, 123
Zenitani S., Hoshino M., 2007, ApJ, 670, 702

APPENDIX A: FIELDS IN A COMOVING FRAME FOR ALIGN CASE

In this appendix, we investigate the particle motion inside and outside the time-dependent current sheet with magnetic field

$$B_y = B_0 \frac{R_{\rm L}}{ct} \tanh\left[\frac{z}{\Delta(t)}\right]. \tag{A1}$$

For the aligned case we consider the same functional form of the time dependence of the sheet thickness on time $\Delta(t) = \Delta_0 (t/t_0)^{\kappa}$. Then, the expression for the electric field

$$E_x = \frac{B_0 R_{\rm L} z}{c^2 t^2} \tanh\left[\frac{z}{\Delta(t)}\right], \tag{A2}$$

$$E_z = 0, \tag{A3}$$

again does not satisfy Maxwell equations for arbitrary κ, and remains valid only for $\kappa = 1$. This corresponds to the linear growth of the sheet thickness due to the radial expansion with constant opening angle of a sheet.

Similar to the orthogonal case there are two possibilities to make the fields satisfy Maxwell equations:

(i) Changing x component of electric field, without any change of z component
(ii) Changing z component without any change of x component.

In contrast to the orthogonal case we change $x$component of the electric field instead of adding E_z one. This implies that Hamiltonian for aligned case will be independent of x:

$$\mathcal{H}^{\rm al} = c\left(m^2c^2 + P_z^2 + p_z^2\right)^{1/2}, \tag{A4}$$

where

$$P_x = p_x - \frac{eB_0 R_L \Delta(t)}{c^2 t} \log\left[\cosh\left(\frac{z}{\Delta(t)}\right)\right]. \tag{A5}$$

Finally, similarly to the orthogonal case, we can find the solution of Maxwell equations by choosing the integration constant such that electric field vanishes at infinity.

$$E_x = \frac{B_0 R_L \Delta(t)}{c^2 t^2}\left\{(1-\kappa)\log\left[2\cosh\left(\frac{z}{\Delta(t)}\right)\right] + \kappa \frac{z}{\Delta(t)} \tanh\left(\frac{z}{\Delta(t)}\right)\right\}. \tag{A6}$$

As a result, an estimation of the current sheet width based on the equality between Larmor radius and the sheet width is still valid for the aligned case. But here the drift leads to the rarefaction of sheet, since it is directed perpendicular to the sheet. On the other hand, since $\partial\mathcal{H}/\partial x = 0$, we have $P_x = \text{const}$. Hence, the particle can gain acceleration along the sheet only due to electromagnetic part of momentum

$$\delta p_x = \frac{eB_0 R_L}{c^2}\left\{\frac{\Delta_0}{t_0}\log\left[\cosh\frac{z_0}{\Delta_0}\right] - \frac{\Delta(t)}{t}\log\left[\cosh\frac{z}{\Delta(t)}\right]\right\} \tag{A7}$$

A1 Particle motion

For aligned current sheet we use expressions (A1), (A3) and (A6) for electric and magnetic fields:

$$B_y = B_0 \frac{t_0}{t} \tanh\frac{z}{\Delta(t)}, \tag{A8}$$

$$E_x = B_0 \frac{R_{\rm L}\Delta(t)}{(ct)^2}\left\{(1-\kappa)\log\left[2\cosh\frac{z}{\Delta(t)}\right] + \kappa\frac{z}{\Delta(t)}\tanh\frac{x}{\Delta(t)}\right\}, \tag{A9}$$

$$E_z = 0. \tag{A10}$$

Here again $\Delta(t) \propto t^{\kappa}$. After writing down equations of motion and some algebra we obtain the following equation for z coordinate of the particle:

$$\ddot{z} = \dot{x}\frac{\Lambda}{t}\tanh\frac{z}{\Delta(t)} \tag{A11}$$

and equality for x component of velocity

$$\dot{x} = v_0 + \Lambda\frac{\Delta_0}{t_0}\ln[2\cosh(x_0/\Delta_0)] - \Lambda\frac{\Delta}{t}\ln[2\cosh(x/\Delta)], \tag{A12}$$

which corresponds to conservation of x component to generalize momentum. After that we should consider three cases:

(i) $\kappa < 1$. In this case, on large time-scales the first term dominates, so we can neglect the second one. The same takes place when $\kappa = 1$ but $\dot{x} \sim \text{const.} \neq 0$
(ii) $\kappa > 1$. In this case, we neglect the first term.
(iii) $\kappa = 1, \dot{x} \to 0$. This scenario is possible if $\Delta \propto t$. In this case $z(t) = z_0(t) + \delta z(t)$, where $z_0/\Delta = \text{const}$. Accordingly, $\delta z \ll z_0$ and $z_0''(t) = 0$.

In the first case we have

$$\ddot{z} = \Lambda\frac{v_0 + V}{t}\tanh(z/\Delta), \tag{A13}$$

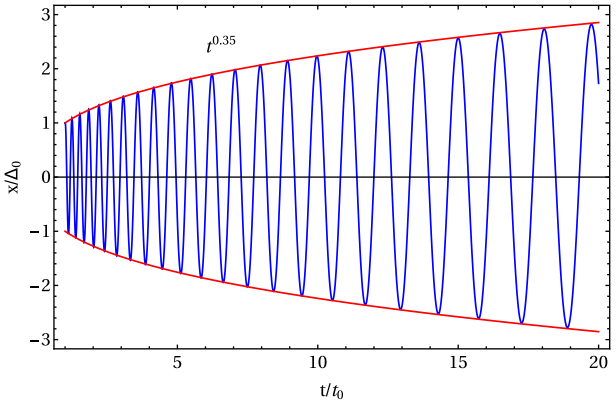

Figure A1. Numerical solution to equation (A13). The self-consistency obtained for $\kappa = 0.35$.

where $V = \Lambda \frac{\Delta_0}{t_0} \ln[2\cosh(x_0/t_0)]$. This equation cannot be solved analytically for arbitrary κ even in $z/\Delta \ll 1$ limit. For $v_0 + V < 0$ the numerical solution of this equation has been shown at (A1).

In the second case we obtain the following equation:

$$\ddot{z} = -\Lambda^2 \frac{\Delta}{t^2} \tanh(z/\Delta) \log[2\cosh(z/\Delta)]. \tag{A14}$$

This equation is similar to equation (78). As we already established above, it describes particle orbit with $t^{1/2}$ radius growth rate.

Finally for $\kappa = 1$ we have

$$\ddot{\delta z} = -\Lambda^2 \frac{\delta z}{t^2} \tanh^2(x_0/\Delta). \tag{A15}$$

The solution of this equation is

$$\delta z \propto \sqrt{t} \cos\left[\Lambda \tanh\left(\frac{x_0}{\Delta(t)}\right) \log t\right]. \tag{A16}$$

This solution describes radial motion of particle experiencing Larmor's motion in declining field.

This paper has been typeset from a TEX/LATEX file prepared by the author.